A NUMERICAL STUDY ON FLOW BOILING WITHIN MICRO-PASSAGES: THE EFFECT OF SOLID SURFACE THERMOPHYSICAL PROPERTIES

Konstantinos Vontas[1*], Francesco Latella[2], Anastasios Georgoulas[1], Nicolas Miché[1], Marco Marengo[1]
*Author for correspondence
[1]Advanced Engineering Centre, School of Computing Engineering and Mathematics,
University of Brighton,
Lewes Road, BN2 4GJ, Brighton, East Sussex, UK

[2]Department of Engineering and Applied Sciences,
University of Bergamo,
Viale Marconi 5, 24044 Dalmine, Italy

E-mail: k.vontas@brighton.ac.uk

ABSTRACT

In the present paper the effect of solid surface thermophysical properties under saturated flow boiling conditions within a considered microchannel is numerically investigated. The simulations are performed by utilising a custom, enhanced VOF-based solver that has been developed in OpenFOAM CFD Toolbox and accounts for conjugate heat transfer between solid and two-phase fluid domains. The properties of stainless steel, copper and silver are considered, utilising a single rectangular microchannel having a hydraulic diameter D_h of 200μm. Due to the high computational cost, a channel length L of only 4.80 mm is used for all cases. The working liquid is ethanol, while the applied heat and mass fluxes are 20 kw/m^2 and 150 kg/m^{2}s, respectively. Two different series of simulations are performed. In the first series the focus is on a single nucleation site and a single nucleation event, tracking the flow path and the growth characteristics of a single bubble. In the second series multiple nucleation sites with four subsequent nucleation events are examined. In the first series, the numerical simulation predictions indicate that the alternation of the solid surface properties, do not affect the resulting bubble dynamics and an elongated vapour slug is formed for all cases. Under the examined conditions, a small difference on the local time-averaged heat transfer coefficient between the different cases is observed, with the silver channel showing the highest (3.93%) and the copper channel showing the lowest (2.55%) increase in the global heat transfer coefficient, compared to the corresponding single-phase values that constitute the initial condition for each case. From the second series of simulations, it is evident that multiple nucleation sites with multiple nucleation events lead to more significant enhancement of the heat transfer coefficient with respect to the reference single-phase cases but also in significant heat transfer performance differences, comparing the different channels to each other.

INTRODUCTION

The rapidly increasing power density of the developed power systems has become an important factor that constrains the further development of electronic products, due to high generation rates of residual heat that needs to be dissipated. The traditional thermal management methods that are used today and are based on air-cooling, cannot sufficiently cope with such high rates of heat fluxes. Conversely, flow boiling within microchannels can provide effective cooling of such high heat generation rates due to the combination of the underpinned latent heat of vaporisation and the considerably larger ratio of surface area to volume. Since the introduction of the microchannel cooling method by Tuckerman and Pease [1], many investigations have been performed in order to study the various factors that influence the thermal performance, and how this can be further enhanced [2–4]. Therefore, aspects such as, surface geometry, aspect ratio, fluid properties, surface wettability and more, have been extensively studied in the past [5–8]. However, among the various influencing factors, the thermophysical properties of the heated solid surface is also considered to play a significant role on thermal performance of micro-passages. In the past years, a number of experimental studies on the flow boiling heat transfer in minichannels and microchannels have been reported. These include the experiments that Bang and Choo [9] carried out, studying the effect of different solid materials on flow boiling heat transfer coefficient. The diameter of the channels was 1.67 mm. The results showed that the flow boiling heat transfer coefficient in a minichannel varies only by heat flux, independent of mass flux and vapor quality. Similar results were reported by [10]. The effect of solid surface thermophysical properties has been studied also in experimental works on the nucleate boiling regime, reporting their significant role on parameters such as heat transfer and pressure drop [11,12].

NOMENCLATURE

c_p	[J/kgK]	Heat capacity
D_h	[mm]	Hydraulic diameter
G	[kg/m^{2}s]	Mass flux
h	[W/m^{2}K]	Heat transfer coefficient
L^*	[-]	Dimensionless length of the channel
q''	[W/m^2]	Heat flux

T	[K]	Temperature

Special characters

α	[-]	Volume fraction ratio
γ	[-]	Bulk fluid properties
$\Delta\bar{h}$	[%]	Percentage difference between two-phase and single-phase simulation of the same surface material
λ	[W/mK]	Thermal conductivity
ν	[m²/s]	Kinematic viscosity
ρ	[kg/m³]	Density
σ	[N/m]	Surface tension

Subscripts

l	Liquid
f	Fluid
l-v	Liquid-vapour interface
int	Interface: between fluid and solid layers
s	Solid surface
sat	Saturation
SP	Single-phase
TP	Two-phase
w	Wall

Some of the most frequently utilised solid surfaces in the industry, include materials such as stainless steel and copper. These surfaces have different thermal properties, and in combination with different parameters such as machinability, corrosion, and wear resistivity are selected accordingly for various applications. In experimental investigations of microchannels that use different materials and aim to study the effect of the thermal properties of the heated solids, the experiments are usually conducted after these surfaces are treated, in order to have the same average roughness (otherwise roughness which is also considered to play significant role in heat transfer, should be taken into account). However, although the roughness difference between the tested surfaces can be minimised by treating the surfaces, other surface characteristics such as surface wettability and boiling inception characteristics can be altered as well, making the process of isolating the effect of solid surface thermophysical properties, a challenging task. Conversely, this can be done by performing numerical simulations on smooth surfaces, where only the solid properties of the tested solid surfaces are changed, keeping other parameters such as roughness, fluid properties and wettability unchanged. Yet still, such numerical investigations are limited in the literature and have not been studied comprehensively.

In the present paper, the effect of surface properties for the case of saturated flow boiling within microchannels is investigated in order to isolate, identify and quantify the effect of thermophysical solid domain properties of the utilised microchannels on the average heat transfer coefficient. Three different solid surfaces are considered by performing 3D conjugate heat transfer, transient numerical simulations, utilising a custom, enhanced VOF-based solver that has been developed in OpenFOAM CFD Toolbox. Both qualitative and quantitative results are reported and discussed, aiming to add valuable insight and understanding regarding the identification and quantification of the proposed effect.

NUMERICAL METHOD

Governing Equations

The numerical experiments performed for the present study, are conducted by utilising the open-source toolbox OpenFOAM, and employing a custom, enhanced Volume OF Fluid (VOF) solver. The enhancements of the proposed solver include a treatment for spurious velocities dampening (a well-known defect of VOF methods), an improved dynamic contact angle treatment to accurately account for wettability effects as well as the implementation of a phase-change model in the fluid domain, accounting for conjugate heat-transfer with the solid domain. In the following paragraphs the governing equations for mass, momentum, energy, and volume fraction are presented. The governing equations shown below are based in the assumption that that liquid and vapour phases are both treated as incompressible, immiscible, Newtonian fluids.

The utilised solver has been extensively validated in the past against various cases of adiabatic and diabatic bubble and droplet dynamics in comparison with available analytical solutions as wells as experimental measurements [13–16].

The mass conservation equation is given as:

$$\nabla \cdot (\rho \vec{U}) = \dot{\rho} \qquad (1)$$

where $\vec{U}$ is the fluid velocity and ρ is the bulk density. The source term on the right-hand side accounts for the phase change. The conservation of momentum is given by the following equation:

$$\frac{\partial}{\partial t}(\rho \vec{U}) + \nabla \cdot (\rho \vec{U}\vec{U}) - \nabla \cdot \left\{ \mu \left[\nabla \vec{U} + (\nabla \vec{U})^{\mathrm{T}} \right] \right\} = -\nabla p + \vec{f}_{\mathrm{ST}} + \vec{f}_{\mathrm{g}} \qquad (2)$$

where p is the pressure and μ is the bulk dynamic viscosity. The momentum source terms on the right-hand side of the equation accounts for the effects of surface tension and gravity, respectively. The surface tension term is modelled according to the classical approach of Brackbill et al.. The conservation of energy balance is given by the following equation:

$$\frac{\partial}{\partial t}(\rho c_p T) + \nabla \cdot (\vec{U}\rho c_p T) - \nabla \cdot (\lambda \nabla T) = \dot{h} \qquad (3)$$

where c_p is the bulk heat capacity, T the temperature field, and λ is the bulk thermal conductivity. The source term on the right-hand side of the equation represents the contribution of the enthalpy of evaporation/condensation or else the cooling/heating associated with the latent heat of the phase-change. The volume fraction α is advected by the flow field by the following equation:

$$\frac{\partial \alpha}{\partial t} + \nabla \cdot (\alpha \vec{U}) - \nabla \cdot (\alpha(1-\alpha)\vec{U}_r) = \frac{\dot{\rho}}{\rho}\alpha \qquad (4)$$

Interface sharpening is very important in simulating two-phase flows of two immiscible fluids. In OpenFOAM the sharpening of the interface is achieved artificially by introducing the extra compression term $\nabla \cdot (\alpha(1-\alpha)\vec{U}_r)$ in Equation (4). $\vec{U}_r$ is an artificial compression velocity. The source term on the right-hand side of the Equation (4) is needed because, due to the local mass source terms, the velocity field is not free of divergence. Finally, the bulk fluid properties γ are computed as the averages over the liquid (γ_l) and vapour (γ_v) phases, weighted

with the volume fraction α, i.e. $\gamma = \alpha\gamma_l + (1-\alpha)\gamma_v$. As mentioned previously, the VOF-based solver that is used in the present investigation has been modified accordingly in order to account for an adequate level of spurious currents suppression. More details on the proposed development and validation as well as on the proposed improved VOF method can be found in the paper by Georgoulas et al [13].

The conservation of energy equation in the solid domains is defined as:

$$\frac{\partial}{\partial t}(\rho_s c_{ps} T) = \nabla \cdot (\lambda_s \nabla T) \tag{5}$$

The coupling at the interface between the solid region and fluid region is achieved iteratively through the following conditions:

$$T_f = T_s, \lambda_f \frac{\partial T_f}{\partial n} = \lambda_s \frac{\partial T_s}{\partial n} \tag{6}$$

where T_f is the temperature at the fluid side of the conjugate heat transfer boundary, T_s is the temperature at the solid side of the conjugate heat transfer boundary, λ_f is the thermal conductivity of the fluid domain and λ_s is the thermal conductivity of the solid domain.

The local heat transfer h(x) coefficient can be calculated from the numerical simulation results as follows:

$$h(x) = \frac{q''}{(T_w(x) - T_{sat})} \tag{7}$$

where x represents the central longitudinal axis of the conjugate heat transfer boundary, q'' is the applied heat flux in W/m² at the bottom surface of the solid domain, $T_w(x)$ is the instantaneous temperature along the middle longitudinal line of the conjugate heat transfer boundary and T_{sat} is the saturation temperature. Further details for the implementation, validation and application for the spurious currents dampening, dynamic contact angle modelling and phase change model can be found in previous works by the present authors' research group [8,13,14].

APPLICATION OF NUMERICAL MODEL

Computational Geometry, Mesh and Boundary Conditions
In the following paragraphs, details regarding the computational geometry, grid and selected boundary conditions are presented. In order to take into account, the transient solid conduction effects within the substrates, the computational domain is necessary to be discretised into two separate parts, the solid domain, where a uniform, constant heat flux is applied at its bottom boundary and the fluid domain which is initially filled with a flowing liquid. After a grid independence study, the optimum cell size that is selected for the numerical investigation is selected to be 2 μm, whereas the total number of cells of the solid and fluid domain is 8.1M and 27M, respectively. More details about the proposed mesh independence study can be found here [17]. The dimensions of the solid domain (length, height and width) are Ls = 4.80 mm, Hs = 0.09 mm, Ws = 0.15 mm, while for the fluid domain are Lf = 4.80 mm, Hf = 0.30 mm, Wf = 0.15 mm. With the exception of the bottom parts of the solid and fluid domain, all the other walls are considered to be adiabatic. At the solid walls, a no-slip velocity boundary condition was used with a fixed flux pressure boundary condition for the pressure values. At the sidewalls of both domains, a zero gradient boundary condition was used for the temperature field. Moreover, a dynamic contact angle boundary condition is imposed for the volume fraction field by assigning the maximum advancing and minimum receding contact angle values from sessile drop measurements, that are then used for the calculation of the dynamic apparent contact angle values during the computations. At the inlet, a constant uniform velocity value, as well as a fixed flux pressure condition was imposed. The volume fraction value was assigned as unity (liquid). As mentioned above, the fluid domain is entirely filled with saturated liquid and the temperature of the liquid at the inlet is also fixed at the saturation temperature. A fixed-value pressure boundary condition and a zero-gradient boundary condition for the volume fraction were used at the outlet, whereas for the velocity values a special (combined) type of boundary condition was used that applies a zero-gradient when the fluid mixture exits the computational domain and a fixed value condition to the tangential velocity component, in cases that the fluid mixture enters the domain. Finally, a zero gradient boundary condition for the temperature field was also prescribed at the outlet boundary. The computational domain and the grid details as well as the utilised boundary conditions are shown in Figure 1.

NUMERICAL SIMULATION SET-UP AND PROCESS
As mentioned above, in order to simulate a realistic case of microchannel heat sink, a conjugate heat transfer model is utilised. The numerical simulations are performed in two main stages. At the first stage, within the microchannel, a liquid is flowing at saturation temperature and with constant uniform velocity from the inlet, whereas in the solid domain, a constant heat flux is applied at its bottom boundary. This stage is ran up for few hundreds of milliseconds until the initial thermal and hydrodynamic boundary layers are fully developed. This first stage is common for both series of numerical simulations that are conducted in the present paper. At the second stage, for the first series of simulations, a small vapour nucleus (bubble seed) represented as a half-sphere with a radius of 20 μm is patched on the conjugate heat transfer boundary (interface between the fluid and solid domains) at a distance of 200 μm from the channel inlet. This is necessary, due to the fact that the utilised model, does not account for nucleation. Once the bubble seed is patched within the previously developed thermal boundary layer, boiling occurs at the meniscus (solid/liquid/vapour triple line) as well as at the parts of the liquid/vapour interface that is in contact with temperatures higher that the saturation temperature. Finally, simulation is continued up to a point where the leading edge of the developed evaporating elongated bubble reaches the outlet of the microchannel. For the second series of numerical simulations, in the second stage of the runs, 30 arbitrary located bubble seeds are positioned on the conjugate boundary representing multiple simultaneous nucleation events. This process is repeated for four subsequent nucleation cycles allowing for a specific waiting time. For all runs, ethanol is selected as the working fluid. The properties of both phases are taken at the saturation equilibrium point for a pressure of $P_{sat} = 1$

bar, which corresponds to a saturation temperature of $T_{sat} =$ 351.05 K (REFPROP NIST software). In more detail, the liquid and vapour densities are $\rho_l = 736.78$ kg/m^3 and $\rho_v = 1.63$ kg/m^3, the liquid and vapour kinematic viscosities are $\nu_l = 6.01 \times 10^{-7}$ m^2/s and $\nu_v = 6.37 \times 10^{-6}$ m^2/s, the liquid and vapour thermal conductivities as $\lambda_l = 0.15$ W/mK and $\lambda_v = 0.02$ W/mK and the liquid and vapour heat capacities are $c_{p,l} = 3182$ J/kgK and $c_{p,v} = 1804$ J/kgK. As for the solid domain, three different solids are employed. In more detail, stainless steel, brass and copper have been considered. The properties of the solid domains as well as the values of the advancing and receding contact angles between ethanol and the corresponding surface are summarised in Table 1. As it can be seen, the contact angle values for all cases are very close with each other and correspond to high hydrophilicity. The very small differences between the contact angle values between
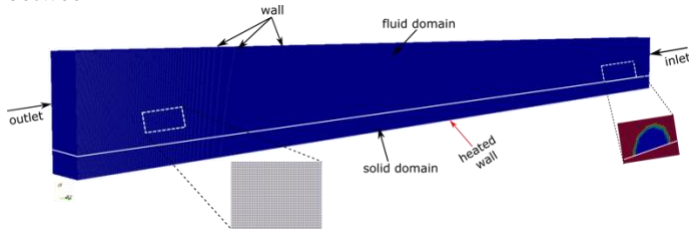
Figure 1: Computational domain, boundary conditions, mesh details and nucleus bubble position at 0ms.

the cases can be considered as an advantage in the present investigation because, it has been shown that variation of surface wettability plays an important role not only in heat transfer rate, but also in general hydrodynamics behaviour of the flow. Hence, these particular solid surfaces were deliberately selected in order to have considerably variable thermophysical properties but at the same time to present similar wettability characteristics with ethanol.

Table 1: Solid domain properties and wettability characteristics.

Case	Solid surface	ρ_s(kg /m^3)	$c_{p(s)}$ (J/ kgK)	λ_s (W/ mK)	θ_a (°)	θ_r (°)
I	Stainless steel	7840	500	16.2	19	8
II	Copper	8933	392	396.8	15	7
III	Silver	10500	235	429	14	7

For the present investigation, three, transient 3D numerical simulations have been performed, with the help of a High-Performance Computing (HPC) cluster. For each of the single-phase simulations (first stage), 200 computational cores have been utilised. As mentioned earlier this is ran up to a few seconds of flow time, with an average computational time for each case of around 20 days. For the subsequent two-phase stage of the simulations, utilising also 200 cores per run, the corresponding calculation duration of each case was about 14 days. Hence, a total of approximately 490,000 core hours were required for these simulations to be finalised. A variable calculation time step was utilised for the two-phase runs with the courant number kept constant at 0.5. Hence the calculation time step was varied

automatically ranging from 10-8 up to 10-6 s. Finally, the uniform applied heat flux at the bottom of the solid domain was fixed to 20 kW/m^2 and the liquid mass flux entering the fluid domain was fixed to 150 kg/m^{2}s, for the present numerical investigation.

NUMERICAL SIMULATION RESULTS

A qualitative comparison between the examined cases can be seen in Fig. 2, where a 2D top view and 3D isometric view of the spatial and temporal evolution of the vapour bubble for the three examined solid surfaces, are depicted. In total four common time instants are shown, as well as the time instant just before the leading edge of the bubble touches the outlet of the channel in each case. In each time instant, the grey surface represents the liquid/vapour interface, while the coloured contours in a clip section that extends from one side of the channel up to its middle plane, reveal the developed temperature fields in both the fluid and solid regions of the computational domain. Overall, it can be seen that for all three cases, similar flow patterns and heat transfer mechanisms are observed. With regards to the spatial evolution of the flow, in the early stages of the bubble growth (up to 2.5 ms) the vapour bubble remains in contact with the heated wall, making contact line evaporation the prevailing heat transfer mechanism, for both cases. However, before the leading edge of the bubble reaches the second half of the channel, the initial bubble that has been transformed into an elongated vapour slug completely detaches from the bottom heated surface enabling liquid film evaporation as the dominant heat transfer mechanism. Similarly, there is no significant contact between the top part of the vapour bubble and the top wall of the channel. Conversely, a complete contact of the channels' sidewalls and the vapour slug can be seen throughout the entire bubble growth process, once the volume of the bubble is big enough to reach the side walls, forming dry patches throughout the entire flow process. Observing the overall bubble volume growth with respect to time for the three cases, it is evident that the variation of the solid domain thermophysical properties, changing the domain material from steel to copper and silver, results to progressively higher evaporation rates that should be expected to result to a corresponding increase in the cooling effectiveness. However, from the temperature contours in the solid domains it is quite evident that the final steel temperatures are a bit lower than copper and silver that present quite similar temperature distribution. This can be attributed to the quite lower thermal diffusivity value of the steel in comparison to copper and silver that results to different transient thermal conduction effects. Therefore, a more quantitative investigation is necessary.

In order to provide a quantitative comparison of the results, the time averaged local Heat Transfer Coefficient (HTC) $\bar{h}(x)$ is plotted against the dimensionless length of the channel L* in Fig.
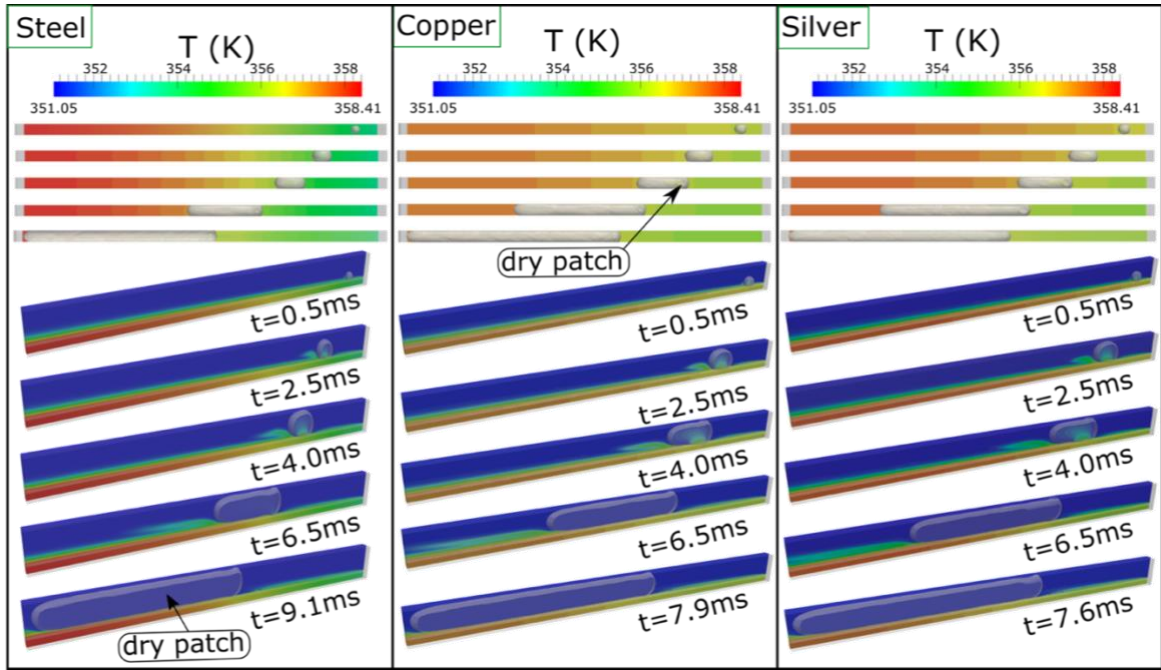
Figure 2: 2D top and 3D side views of qualitative results for single bubble growth for stainless steel (left) and copper (middle) and silver (right) for four common time periods and the last time period before the bubble reaches the outlet.
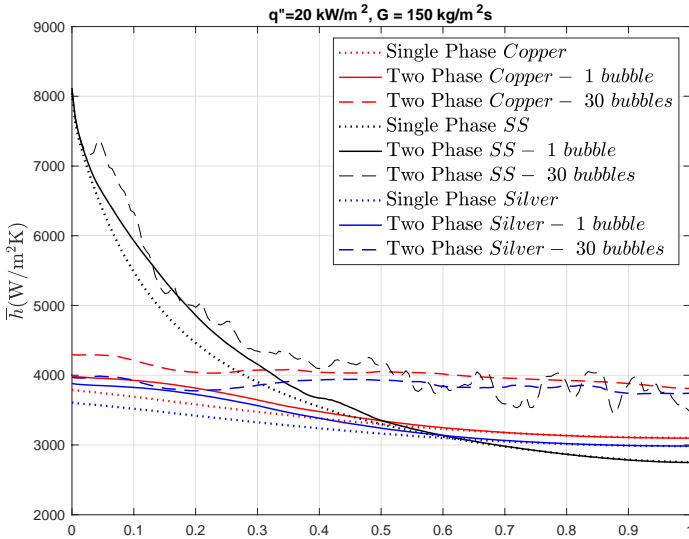
Figure 3: Time-averaged local heat transfer coefficient $\overline{h}$ over L^* for single and two-phase runs.

3. It should be mentioned that for each case the corresponding single-phase curve from the first stage of each run is also plotted as a reference curve in order to quantify the increase in the variation of the local heat transfer coefficient due to the passage of the generated vapour bubble. Also results from the second series of simulations with the multiple nucleation sites and multiple nucleation events. From the results, it is evident that the different solid surface material properties have resulted in different $\overline{h}(x)$ distributions. In more detail, focusing first on the single-phase reference curves it is evident that stainless steel presents quite higher values of heat transfer in the first half of the channel with respect to copper and silver that show quite similar values. In each case comparing the single-phase curves with the two different two-phase curves (single nucleation site with single nucleation event and multiple nucleation sites with four subsequent nucleation events) it is evident that the passage of the single bubble creates a slight increase in the local HTC in comparison to the single-phase reference curves. This increase is more significant when more realistic cases with multiple nucleation sites and multiple nucleation events are simulated.

Figure 4 shows the local time-averaged percentage difference between the single-phase and the two-phase simulations ($\Delta\overline{h} = [((\overline{h}_{TP} - \overline{h}_{SP})/ \overline{h}_{SP})\times100]$). As can be seen, also from this graph, for the single nucleation site and single nucleation event cases the curves of silver and copper show similar distributions with the silver channel performing slightly better. However, the resulting curve of the stainless steel channel shows a quite different distribution. It is worth mentioning that for all three surfaces, the highest local difference value of $\Delta\overline{h}$ between single-phase and two-phase runs is approximately at $L^*=0.15$. Considering now the multiple nucleation sites with multiple nucleation events cases the stainless steel and silver channel curves show a similar distribution while the copper case shows a more irregular trend with a lot of subsequent maxima and minima.

In order to check the overall performance in each case the global heat transfer coefficient for the cases with multiple nucleation sites and four subsequent nucleation events is calculated for the three different channels (i.e. stainless steel, copper and silver) by taking the area under the corresponding curves of Figure 3. These are summarised in Table 2. As it can be seen the stainless-steel channel has the highest heat transfer performance followed by the copper and the silver channels. In more detail the stainless-steel channel results in a global HTC that is 16% higher than the silver channel and 11% higher that the copper channel.

Table 2: Global heat transfer coefficients for each channel material, considering the second series of numerical simulations with multiple nucleation sites and recurring nucleation events .

Material	Single-phase	Two-phase 30 bubbles
	$\bar{h}_{global}$ (-)	$\bar{h}_{global}$ (-)
Copper	3352	4025
Stainless steel	3742	4471
Silver	3211	3856
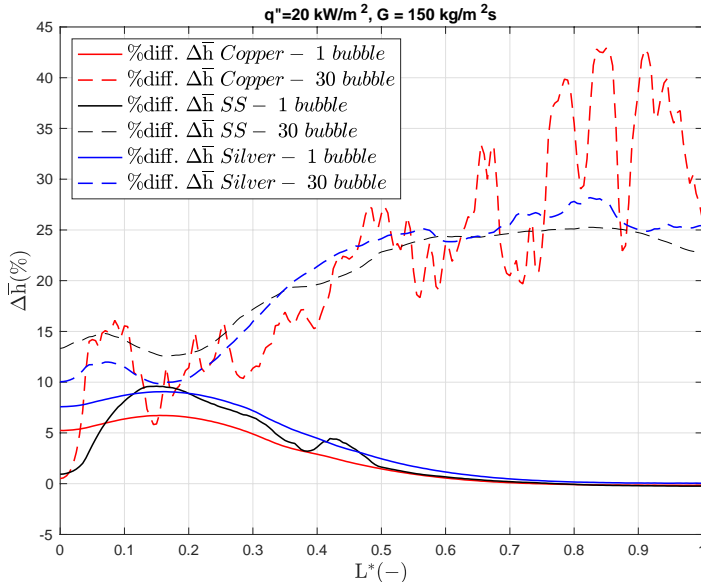
Figure 4: Percentage difference between two-phase and single-phase time averaged $\bar{h}$ over L*, for the three examined cases.

CONCLUSIONS

A numerical investigation on the effect of thermophysical properties of the solid heated domain in the flow boiling characteristics within a rectangular microchannel is presented in the present paper. The mass flux considered is 150kg/m^{2}s, whereas a constant and uniform heat flux of 20kW/m^2 is applied at the bottom side of the solid domain. Flow visualizations on single nucleation events indicate that under the examined conditions, the effect of the solid surface properties have a minor influence on the developed two-phase flow patterns. However, for more realistic cases with 30 simultaneous nucleation events it is evident that by altering only the solid domain properties the time averaged heat transfer coefficient is enhanced up to 16% even at the early transient stages of the two-phase flow development within the first few milliseconds from the nucleation events. Finally, a general conclusion is that the utilised direct numerical simulation methodology can constitute a valuable tool for identifying and quantifying the effects of fundamental controlling parameters in the bubble dynamics and heat transfer characteristics in the case of flow boiling within micro-passages.

REFERENCES

[1] D.B. Tuckerman, R.F.W. Pease, High-Performance Heat Sinking for VLSI, IEEE Electron Device Lett. EDL-2 (1981) 126–129. https://doi.org/10.1109/EDL.1981.25367.

[2] J.R. Thome, Boiling in microchannels: A review of experiment and theory, Int. J. Heat Fluid Flow. 25 (2004) 128–139. https://doi.org/10.1016/j.ijheatfluidflow.2003.11.005.

[3] S.G. Kandlikar, Scale effects on flow boiling heat transfer in microchannels: A fundamental perspective, Int. J. Therm. Sci. 49 (2010) 1073–1085. https://doi.org/10.1016/j.ijthermalsci.2009.12.016.

[4] J.R. Thome, A. Cioncolini, Flow Boiling in Microchannels, Adv. Heat Transf. 49 (2017) 157–224. https://doi.org/10.1016/bs.aiht.2017.06.001.

[5] D.F. Sempértegui-Tapia, G. Ribatski, The effect of the cross-sectional geometry on saturated flow boiling heat transfer in horizontal micro-scale channels, Exp. Therm. Fluid Sci. 89 (2017) 98–109. https://doi.org/10.1016/j.expthermflusci.2017.08.001.

[6] M. Andredaki, K. Vontas, A. Georgoulas, N. Miché, M. Marengo, Effect of Channel Aspect Ratio on Flow Boiling Characteristics within Rectangular Micro-passages, in: Proc. 5th World Congr. Momentum, Heat Mass Transf., Lisbon, 2020: pp. 1–8. https://doi.org/10.11159/icmfht20.147.

[7] T. Harirchian, S. V. Garimella, Effects of channel dimension, heat flux, and mass flux on flow boiling regimes in microchannels, Int. J. Multiph. Flow. 35 (2009) 349–362. https://doi.org/10.1016/j.ijmultiphaseflow.2009.01.003.

[8] K. Vontas, M. Andredaki, A. Georgoulas, N. Miché, M. Marengo, Wettability effect on flow boiling characteristics within micro-passages, Proc. 5th World Congr. Momentum, Heat Mass Transf. (2020) 1–9. https://doi.org/10.11159/icmfht20.149.

[9] K.H. Bang, W.H. Choo, Flow boiling in minichannels of copper, brassm and aluminium round tubes, in: ICMM2004 2nd Int. Conf. Microchannels Minichannels, Rochester, NY, 2004: pp. 1–6. https://doi.org/10.1115/ICMM2004-2381.

[10] A.H. Al-Zaidi, M.M. Mahmoud, T.G. Karayiannis, Flow Boiling of HFE-7100 in Multi-Microchannels: Effect of Surface Material, in: Proc. 5th World Congr. Momentum, Heat Mass Transf., Lisbon, 2020: pp. 1–5. https://doi.org/10.11159/icmfht20.124.

[11] L. Zou, B.G. Jones, Heating surface material's effect on subcooled flow boiling heat transfer of R134a, Int. J. Heat Mass Transf. 58 (2013) 168–174. https://doi.org/10.1016/j.ijheatmasstransfer.2012.11.036.

[12] R. Hosseini, A. Gholaminejad, M. Nabil, M.H. Samadinia, Concerning the effect of surface material on nucleate boiling heat transfer of R-113, in: ASME/JSME 2011 8th Therm. Eng. Jt. Conf. AJTEC 2011, Hawai, USA, 2011: pp. 1–6. https://doi.org/10.1115/ajtec2011-44498.

[13] A. Georgoulas, P. Koukouvinis, M. Gavaises, M. Marengo, Numerical investigation of quasi-static bubble growth and detachment from submerged orifices in isothermal liquid pools: The effect of varying fluid properties and gravity levels, Int. J. Multiph. Flow. 74 (2015) 59–78. https://doi.org/10.1016/j.ijmultiphaseflow.2015.04.008.

[14] K. Vontas, M. Andredaki, A. Georgoulas, K.S. Nikas, M. Marengo, Numerical Investigation of Droplet Impact on Smooth Surfaces with Different Wettability Characteristics: Implementation of a dynamic contact angle treatment in OpenFOAM., Proc. ILASS–Europe 2017. 28th Conf. Liq. At. Spray Syst. (2017) 6–8. https://doi.org/10.4995/ILASS2017.2017.5020.

[15] A. Georgoulas, M. Andredaki, M. Marengo, An enhanced VOF method coupled with heat transfer and phase change to characterise bubble detachment in saturated pool boiling, Energies. 10 (2017). https://doi.org/10.3390/en10030272.

[16] K. Vontas, C. Boscariol, M. Andredaki, A. Georgoulas, C. Crua, J.H. Walther, M. Marengo, Droplet Impact on Suspended Metallic Meshes: Effects of Wettability, Reynolds and Weber Numbers, Fluids. 5 (2020) 1–28. https://doi.org/10.3390/fluids5020081.

[17] K. Vontas, M. Andredaki, A. Georgoulas, N. Miché, M. Marengo, The effect of surface wettability on flow boiling characteristics within microchannels, Int. J. Heat Mass Transf. 172 (2021). https://doi.org/https://doi.org/10.1016/j.ijheatmasstransfer.2021.121133.